Progress In Electromagnetics Research B, Vol. 35, 29–51, 2011

DESIGN AND IMPLEMENTATION OF A PLANAR 4×4 BUTLER MATRIX IN SIW TECHNOLOGY FOR WIDE BAND HIGH POWER APPLICATIONS

T. Djerafi[1], N. J. G. Fonseca[2,*], and K. Wu[1]

[1]Poly-Grames Research Center, École Polytechnique de Montréal, Montréal, QC H3T 1J4, Canada

[2]Antenna Department, French Space Agency (CNES), 18 av. Edouard Belin, 31401 Toulouse cedex 9, France

Abstract—This paper introduces a novel design of Butler matrix in substrate integrated waveguide (SIW) technology with wide frequency band characteristics. Butler matrices are particularly useful in advanced antenna design and characteristics such as wideband operation, power handling, manufacturing, integration, cost, etc. are typical issues to be addressed in many applications. The proposed planar 4×4 Butler matrix provides an interesting solution to most of these issues. Wideband operation is achieved thanks to improved cross-couplers. These components are also characterized by higher power handling when compared to E-plane couplers. The use of SIW technology enables to reduce insertion losses compared to other printed technologies, while maintaining most advantages of such technologies such as high integration, manufacturing simplicity, low weight, etc. The proposed design is fully described, from the elementary building blocks to the full assembly performances. The design is optimized for operation in Ku-band with a center frequency at 12.5 GHz. A prototype of the 4×4 Butler matrix is manufactured, and good performances are confirmed over 24% relative frequency bandwidth. Potential use of this sub-system in multibeam antenna design is also discussed.

Received 20 June 2011, Accepted 30 September 2011, Scheduled 7 October 2011

* Corresponding author: Nelson J. G. Fonseca (nelson.fonseca@esa.int), now with Antenna and Sub-Millimetre Wave Section, European Space Agency, Keplerlaan 1, 2200AG, Noordwijk, The Netherlands.

1. INTRODUCTION

Multiple beam forming networks (M-BFN) are an important sub-system in advanced antenna design. Their main functionality is to generate multiple beams from a same radiating aperture. Assuming an M-BFN fed array antenna operating in transmitting mode, each output port of the M-BFN is connected to a radiating element of the array antenna while each input port of the M-BFN is associated to one specific beam. One potential use of this multiple beam configuration is space division multiplexing access (SDMA): several users can communicate through the same base station with the same frequency channel provided that they are not located in the same beam and interference levels are controlled. This naturally increases the system capacity and can be conveniently combined with TDMA, FDMA or CDMA [1, 2]. In association with a switch matrix, a multiple beam antenna can also be used for electronic beam steering, replacing mechanical beam steering in radar applications [3]. Switched-beam antennas can also be used in on-board high data rate downlink systems for satellite applications demanding minimal perturbation of the satellite attitude during the mission [4]. When operating in transmit, the M-BFN may be required to handle high power levels. This is also the case when the M-BFN is used in multi-port amplifier (MPA) design. This sub-system is composed of two similar multiple port networks with amplifiers in between [5]. This specific configuration enables to distribute each signal to be amplified among all the amplifiers available. This has two advantages: it minimizes the impact of one amplifier's failure and balances the power operating point of each amplifier, resulting in improved overall efficiency. Accordingly, there is a need to develop highly integrated M-BFNs with high power handling as well as wide band operation, in particular for satellite telecommunication applications in Ku and Ka-band.

Several beam formers are available in the literature and can be separated into two major design families: quasi-optic and circuit designs. The quasi-optic family includes bootlace lenses, such as the Ruze and Rotman lenses [6–8], but they usually suffer from low efficiency due to spillover losses and high coupling between adjacent ports, which make them less suitable for high power applications. Circuit beam formers, or beam forming networks (BFN), are based on combinations of guided wave structures such as directional couplers and phase shifters [9]. Depending on the topology and the signal distribution performed by the BFN, specific losses may be necessary for proper operation. This is for example the case in Blass matrices, requiring dissipation loads at the end of each feeding line to produce

a traveling-wave mode [10]. Such losses are usually not adequate for high power operation, as it may result in thermal dissipation issues. In fact, it was demonstrated that theoretically lossless BFN imposes strong constraints on the signal distribution, which must be orthogonal in multiple beam configuration [11, 12]. The Butler matrix is a well-known implementation of such an orthogonal BFN [13]. The Butler matrix in its standard form is a parallel distribution of the power provided at each beam port through balanced (3 dB) directional couplers. For M-BFN applications, specific phase shifters are required to produce an arithmetic phase progression per beam port resulting in a specific beam pointing direction per beam port. These phase shifters are not required for MPA applications. The Butler matrix without phase shifters is often referred to as the hybrid matrix.

Although general design procedures are available for Butler matrices with a number of beam ports equal to any integral power of two [14], most designs proposed in the literature are limited to 4 beam ports. The schematic design of a 4×4 symmetrical Butler matrix is reported in Figure 1. The matrix is composed of four 3 dB/90° directional couplers and two 45° phase shifters. Two additional crossovers are needed when the matrix is to be integrated in the same plane as the radiating elements forming a fully integrated multibeam linear array antenna. Several Butler matrix designs in planar technologies are proposed in the literature [15–17] but they

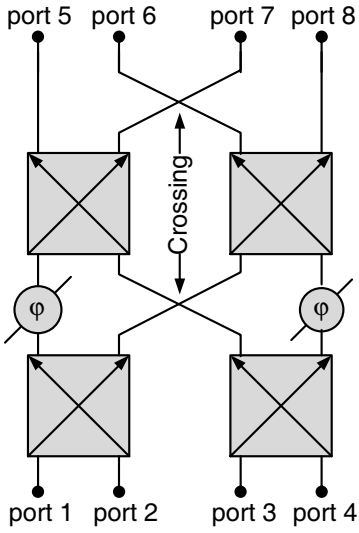

Figure 1. General block diagram of a symmetric 4×4 Butler matrix.

most often suffer from high insertion losses and are not suitable for high power applications. Waveguide technology is usually preferred to improve power handling, but resulting designs are often bulky and their integration is less convenient. This last decade, a new technology, called substrate integrated waveguide (SIW), has been developed with validation at component level [18–28] and application to M-BFN design [29–32] as it combines advantages of planar and waveguide technologies. SIW technology is an excellent compromise to build a Butler matrix when compared to microstrip or waveguide technologies in terms of reduced weight and insertion losses. But designs available so far are often limited in frequency bandwidth. A recent design exhibits a 20% relative frequency bandwidth at Ku-band, but the proposed multi-layer design, based on E-plane couplers, is expected to have limited power handling due to the use of narrow coupling slots [32].

This paper proposes and details the realization of a planar wideband 4×4 Butler matrix in SIW technology with improved power handling thanks to a single layer design approach and wide coupling sections. The paper is organized as follows. The design of the constituting components is first described, including a 3 dB H-plane coupler, a crossover, and phase shifters. A cruciform SIW 90° coupler with improved bandwidth is proposed, and its design considerations and optimization are presented. The performances of the coupler are validated through fabrication and measurement of the optimized design. This coupler is cascaded in a compact form to produce the crossover function. Power handling capability is discussed at component level. The complete matrix is then designed for operation in Ku-band (center frequency set at 12.5 GHz), fabricated and measured. Simulation and measurements are found in good agreement. Radiation performances are finally investigated in the last section.

2. BUILDING BLOCKS DESIGN DESCRIPTION

The different building blocks of the proposed planar Butler matrix are designed on a Rogers RT/Duroid 5870 substrate with a dielectric constant of 2.33 and a substrate thickness of 0.787 mm. As already mentioned, a Butler matrix is composed of balanced hybrid couplers, 0 dB couplers (cross-overs) and phase shifters. A commercial finite element method (HFSS) package is used to optimize the electromagnetic performances of the different building blocks. An equivalent conventional waveguide structure is first optimized and then converted into its SIW counterpart following some design rules as found in [19]. This procedure enables to significantly reduce the structure

meshing complexity and speeds up the optimization process. The next sub-sections describe the different elementary components required for the proposed planar 4×4 Butler matrix.

2.1. Planar 3 dB/90° Hybrid Coupler

Planar balanced SIW directional couplers have been investigated by many authors [23–26]. Some of these couplers are based on the concept of narrow-wall aperture coupling [23, 24]. The coupling is adjusted by the length of the common aperture. In [24], a relative bandwidth of 12% is achieved with limited isolation. Waveguide steps are used to improve the input matching in [23], resulting in a 25% bandwidth. Another type of H-plane coupler design called cruciform directional coupler has been investigated in [25]. Isolation below -20 dB and accurate 90° phase shift between the direct and coupled ports are achieved over 18% bandwidth. In the same order of magnitude, a quasi optical coupler is proposed in [26]. A grating structure is used as mirror in the diagonal section to control the division of the signal. This coupler reaches 20% of relative bandwidth.

E-plane couplers are also available in SIW technology with potentially wider frequency band characteristics [27, 28], but the use of coupling slots (resonant narrow slots usually) or holes (with typically rectangular or elliptical shapes) are known to introduce strong voltage magnification (field strength normalized to the input field) in the coupling zone thus resulting in limited power handling, according to standard multipaction design rules based on the parallel-

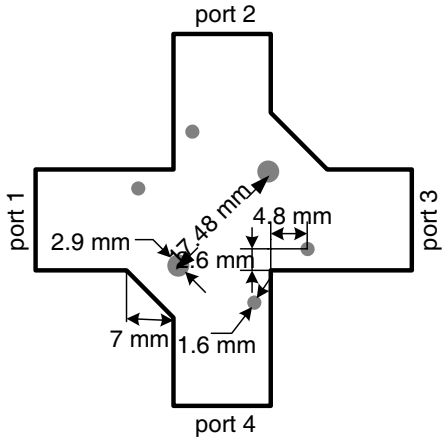

Figure 2. Cruciform H-plane 3 dB/90° hybrid coupler.

plate assumption [33]. In practice, fringing fields generated around slots tend to significantly increase the voltage necessary to induce multipactor [34]. But a proper evaluation of the component's power threshold imposes a specific multipaction analysis. For this reason, slots or holes are usually avoided in high power-handling designs. *E*-plane couplers also require dual- or multi-layer design which introduces potential misalignment errors and increased manufacturing complexity compared to planar designs.

The SIW *H*-plane cruciform directional coupler topology was selected as it is well adapted for planar realizations [25]. The coupling region consists in the crossing area of two simple SIW transmission lines with two via that produce the desired directional properties. Smaller via are used at each port to improve the matching. In this paper, we introduce an improved version of this coupler that exhibits wider bandwidth behavior with a widened cross junction as shown in Figure 2. The optimized dimensions for operation in Ku-band with a center frequency at 12.5 GHz are provided in Figure 2. Simulated *E*-field distribution along the coupler when fed at one of the two input ports is shown in Figure 3. Field distribution remains smooth along the coupler, without local high voltage magnification. This characteristic, combined with the good power handling capability of SIW (up to 450 W at 10 GHz for SIW interconnects and transmission lines) when compared to other printed technologies [35], is expected to allow for high power operation.

The coupler is fabricated and measured. The photography of the corresponding prototype is reported in Figure 4. The simulated and

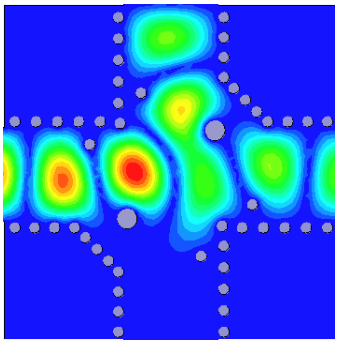

Figure 3. Simulated *E*-field magnitude distributions obtained by HFSS at 12.5 GHz, along the coupler.

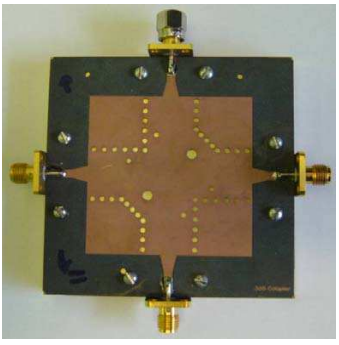

Figure 4. Manufactured 3 dB/90° hybrid coupler.

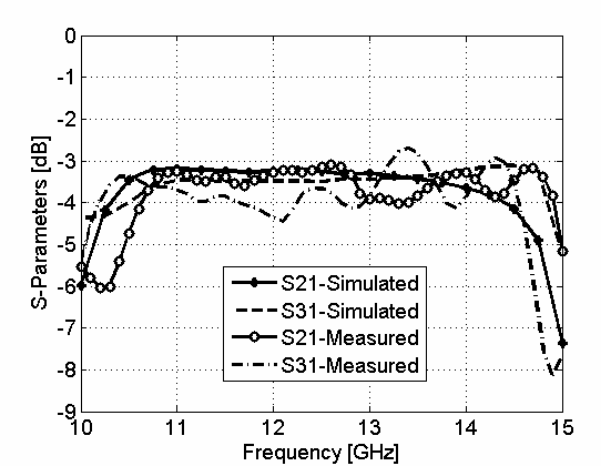

Figure 5. Simulated and measured S-parameters of the manufactured 3 dB coupler: coupling parameters.

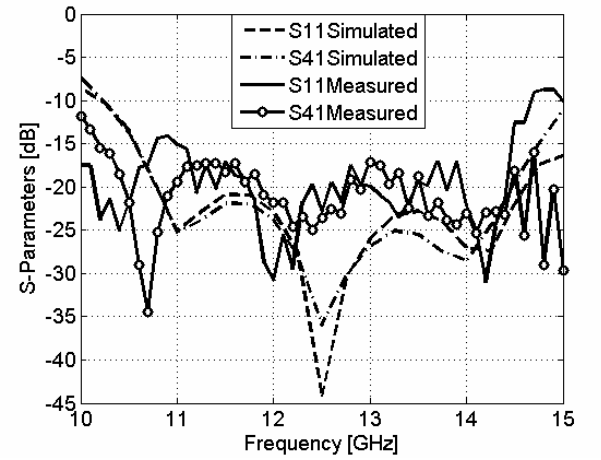

Figure 6. Simulated and measured S-parameters of the manufactured 3 dB coupler: return losses and input ports isolation.

measured scattering parameters are given in Figures 5 and 6. Direct and coupled transmit coefficients are centered at -3.25 dB. Around this value, a dispersion of ± 0.25 dB is observed over the frequency range 10.75–14.2 GHz. This frequency range is defined to reach ports matching and isolation levels better than -20 dB. This frequency

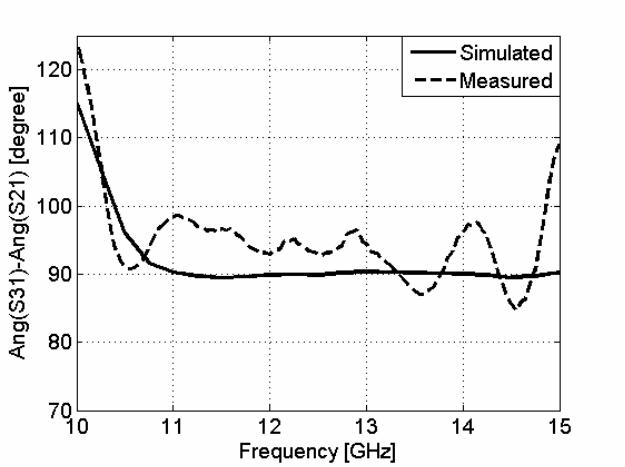

Figure 7. Simulated and measured S-parameters phase difference between direct and coupled ports of the manufactured coupler.

range represents a 28% relative bandwidth, which is excellent for wide band applications especially considering that this improved design has little impact on the overall coupler dimensions. These results are slightly degraded in measurements, but return loss and isolation remain better than 15 dB. Furthermore, impact of interconnects for measurements purposes added to the nominal design is more evident in small structures like this one, which may explain for a certain extent the deviation observed. Figure 7 illustrates simulated and measured relative phases between direct and coupled transmit coefficients, which indicates a 5° peak-to-peak dispersion from the theoretical 90° across the entire frequency band of 10.75–15 GHz. These figures show the good agreement between the experimental results and EM simulations.

2.2. Cross-over (0 dB Coupler)

The crossover is a four port junction crossing two transmission lines in a planar design with proper isolation between the two lines. With notations defined on Figure 8, a cross-over is such that the incoming signal at port 1 is directed towards the output port 3, while signal incoming at port 4 is directed towards output port 2. Such a junction

is defined by the following S-parameters matrix:

$$S = \begin{vmatrix} 0 & 0 & j & 0 \\ 0 & 0 & 0 & j \\ j & 0 & 0 & 0 \\ 0 & j & 0 & 0 \end{vmatrix} \tag{1}$$

A convenient design approach for this component is to cascade two 3 dB couplers, as illustrated in Figure 8. This design is known to provide high isolation between the two crossing transmission lines [36], and resulting relative bandwidth is equivalent to that of the elementary coupler. Starting from the 3 dB coupler described in the previous section, the cross-over design was improved to reduce the overall component's size, as illustrated in Figure 9 with the equivalent waveguide models. To do so, corresponding parts of the two cascaded couplers are merged, resulting in a length reduction of about 30%. More precisely, two inductive posts required to set the coupling and

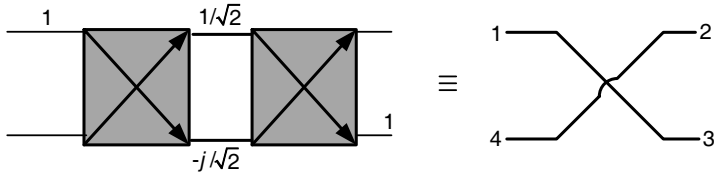

Figure 8. Schematic representation of a 0 dB coupler based on two cascaded 3 dB/90° couplers.

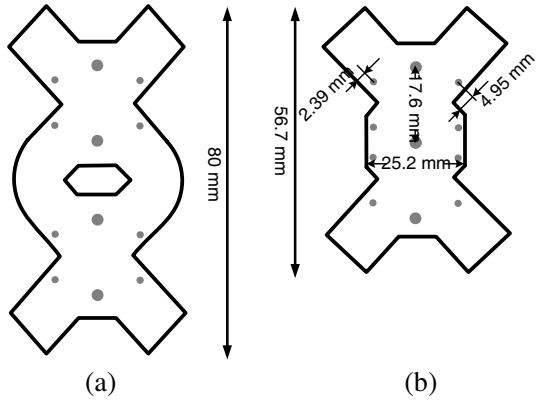

Figure 9. Proposed crossover in equivalent rectangular waveguide model with its geometrical parameters: two cruciform couplers cascaded in (a) regular and (b) compact version.

directional properties of the couplers are merged into a common central inductive post. Flexibility on the inclination of the ports at coupler level is also enabling such a compact design with 45° bends directly at couplers' common ports level. This waveguide model is then translated into its SIW counterpart as illustrated in Figure 10. The field distribution achieved in simulation along the proposed crossover is also reported in Figure 10. Field distribution is very similar to that of the 3 dB coupler despite the compact arrangement, resulting in low voltage magnification as well, suitable for high power operation.

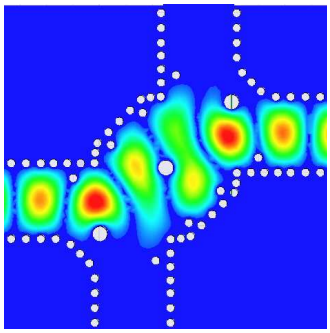

Figure 10. Simulated E-field magnitude distributions obtained by HFSS at 12.5 GHz, along the crossover.

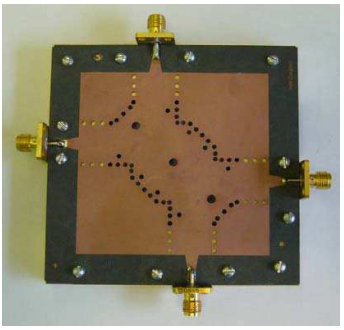

Figure 11. Manufactured 0 dB coupler.

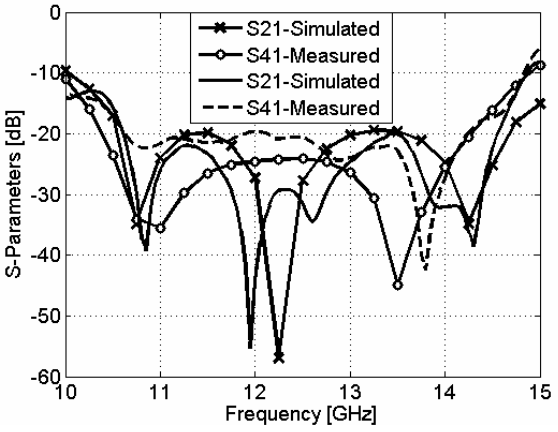

Figure 12. Simulated and measured S-parameters: isolations.

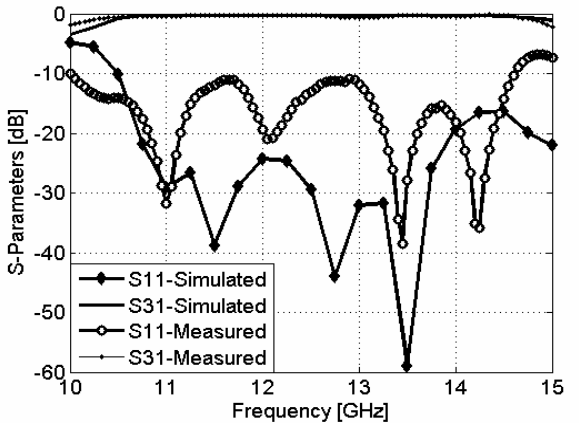

Figure 13. Simulated and measured S-parameters: return loss and transmission.

The photograph of the fabricated prototype is shown in Figure 11. Measured parameters are illustrated in Figures 12 and 13. They are compared with simulated results for the proposed crossover around the frequency band of interest. The measured isolation between input ports (1 and 2) as well as between the input port and crossing output ports (1 and 4) is better than 20 dB over the bandwidth 10.7–14.2 GHz, confirming simulation results. The measured return loss is below -10 dB over the same frequency band, although simulations were predicting values below -20 dB over most of this frequency band. The transmit coefficient from port 1 to port 3 has a worst case value of -0.6 dB over the 11–14 GHz frequency range. Part of measured insertion loss originates from reflection higher than expected at the input port. However, the transmission loss is principally attributed to dielectric loss. Simulated and measured results show that this crossover has a very good performance with a broad bandwidth, ranging from 11 to 14 GHz. Acceptable performances are even reached over the extended 10.5–14.6 GHz frequency range. Over this extended bandwidth, the proposed junction provides insertion loss better than 1 dB and the isolation between ports 1 and 4 better than 20 dB. The same level of isolation is also observed between the two input ports (1 and 2). For comparison, the coupling length of the cross coupler proposed in [29] is $l = 20.17$ mm (limited to the common section) using a substrate with dielectric constant of 2.17 at 26 GHz ($l/\lambda = 2.57$) and show good results over 1 GHz (relative bandwidth of 3.8%). With the proposed design, the coupling length is $l = 32.32$ mm

for a center frequency of 12.5 GHz, resulting in a coupling length normalized to the wavelength of $l/\lambda = 2.05$. The proposed design achieves good performances over a relative bandwidth of 24%, resulting in a design improving the state-of-the-art in both compactness and RF performances.

2.3. Phase Shifters

The phase shifting is implemented using transmission line. To better integrate the proposed beam former with an array antenna, the output ports must be aligned. Consequently, curved transmission lines are used to produce simultaneously adequate output ports position and proper phase delay equivalent to the insertion phase of the crossover

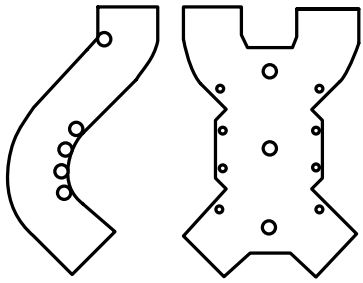

Figure 14. Proposed wide band 0° phase shifter.

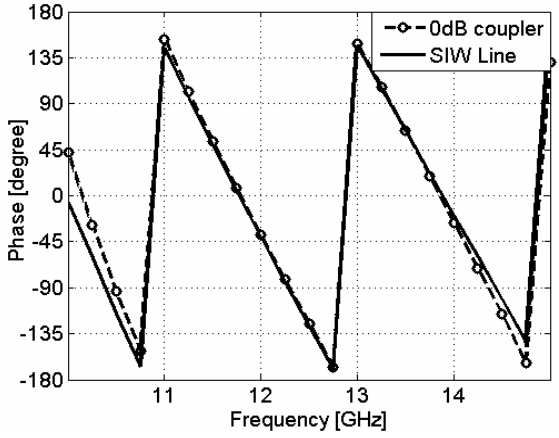

Figure 15. Comparison between the proposed SIW line and 0 dB coupler.

(0° phase shifter). When a simple line is used, the phase difference between the crossover path and the SIW line path has an important variation of about ±30° over the considered frequency range. In fact the phase delay variation versus frequency generated by the crossover is non-linear. This type of variation is caused by the several via in the crossover design, the waveguide width variations and bends. Figure 14 shows the added discontinuities to the curved SIW line to have equivalent perturbation. Simulation results presented in Figure 15 indicate that the phase difference between the crossover path and the SIW line path is better than 5° with the modified transmission line design. The 45° phase shifts required in relation to the first crossover can be designed in a similar manner and with comparable performances.

3. BUTLER MATRIX DESCRIPTION AND PERFORMANCES

To reduce the simulation time, the structure was initially designed using an equivalent rectangular waveguide model shown in Figure 16. As already described, the proposed eight-port network is a combination of four SIW couplers and two crossovers presented in the previous section. These components are connected with two 45° phase delays and two 0° phase delays also presented in the previous section. After validating performances of the continuous walls design, the network is translated to its via-holes counterpart. The via-holes are manufactured first using a mechanical process and then metalized to ensure good connectivity.

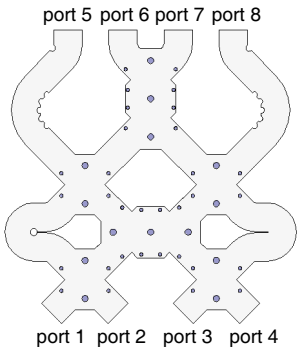

Figure 16. Topology of SIW Butler matrix in equivalent waveguide configuration.

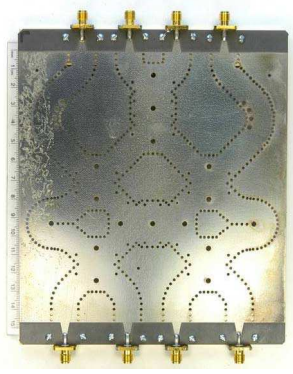

Figure 17. Manufactured planar Butler matrix.

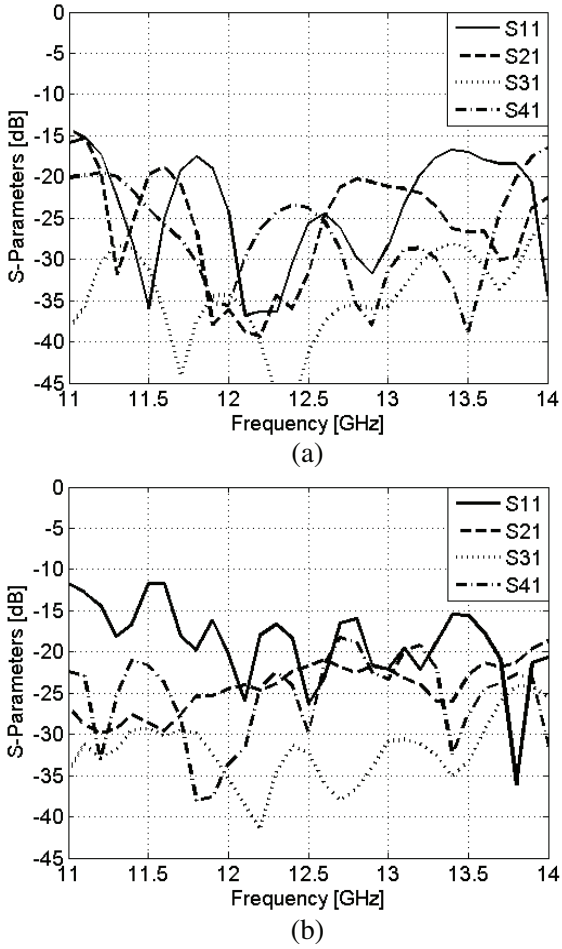

Figure 18. (a) Simulated and (b) measured return loss of the port 1 and isolation toward the other input ports.

Figure 17 is a photograph of the proposed 4×4 matrix. The board is 144 mm by 145 mm. SIW-to-microstrip transitions [19] are added at each circuit port for measurement purpose. The different building blocks can easily be identified. This configuration is less compact than the one described in [29] but the proposed design is intended to avoid the potential diaphonic phenomena caused between two adjacent SIW waveguides sharing a common via-holes line.

Figure 18 shows the return loss and isolations at the input port 1

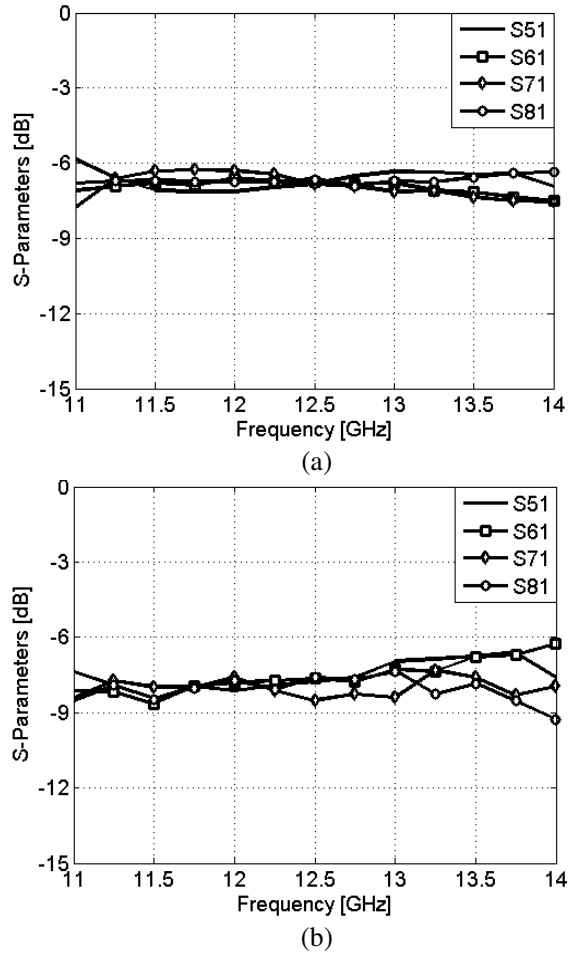

Figure 19. (a) Simulated and (b) measured amplitude distribution of the 4×4 Butler matrix when fed at port 1.

over the frequency range of 11–14 GHz. The isolations are close to our goal of 20 dB, while the return loss is below -15 dB. Overall, the simulated and measured results are in good agreement with small degradation in the measured return loss.

Figures 19 and 20 present simulated and measured amplitude of the transmit coefficients when the matrix is fed at port 1 and port 2 respectively. Good agreement is also found for these parameters between simulation and measurements and results are close to the theoretical value of -6.02 dB over the operating frequency band,

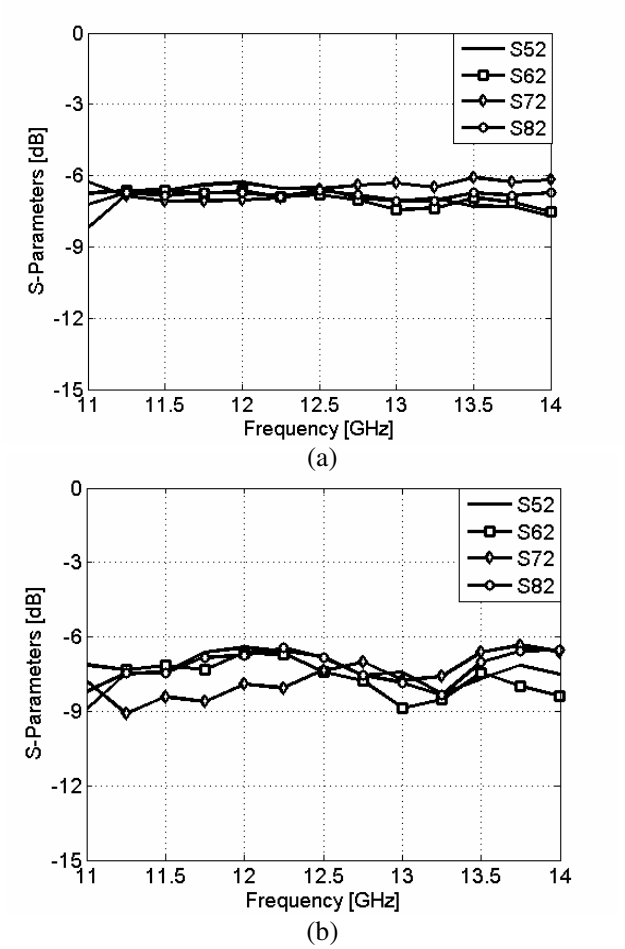

Figure 20. (a) Simulated and (b) measured amplitude distribution of the 4×4 Butler matrix when fed at port 2.

corresponding to an equi-amplitude distribution. The coupling factors are well equalized around -6.75 dB in simulation and around -7.5 dB in measurement. Part of these additional losses is due to the added transitions (not included in the simulation) and substrate losses higher than expected. Proper substrate model calibration should lead to better match between simulation and measurements. Still, insertion losses remain acceptable considering the operating frequency and the number of components chained. Owing to the matrix's symmetry, one can expect performances for ports 3 and 4 to be very similar, although not presented in this paper.

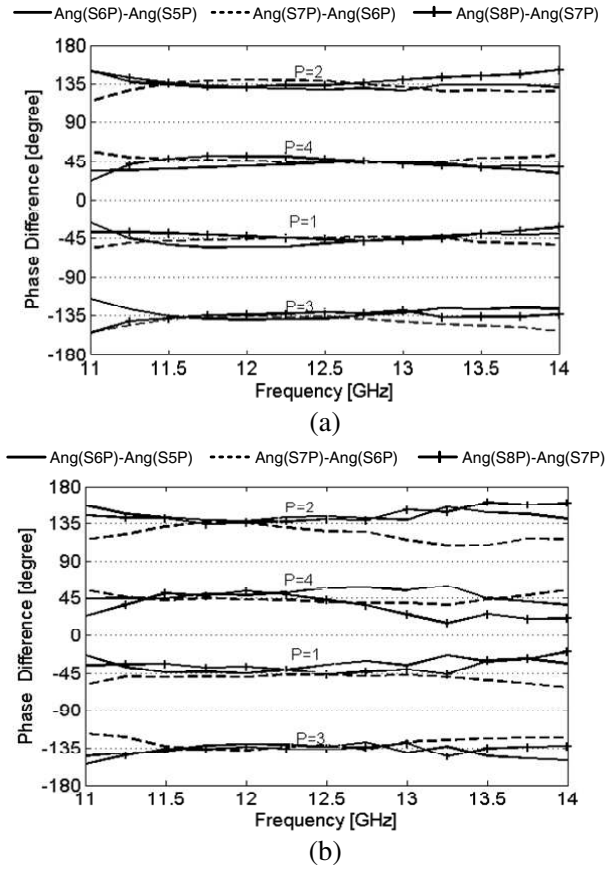

Figure 21. (a) Simulated and (b) measured output phase distribution per input port.

The theoretical relative phase progression between adjacent output ports is $-45°$, $+135°$, $-135°$, and $+45°$ when the signal is incoming at input ports 1, 2, 3 and 4 respectively. Figure 21 shows simulation and measured phase differences for the 4 input ports. The simulated phase differences between different output ports when the signal is fed at each input port are $-45° \pm 10°$, $135° \pm 15°$, $-135° \pm 15°$ and $45° \pm 10°$ over the frequency range. Measurements degradation is observed after 13 GHz. Port 2 and port 4 have slightly degraded performances compared to the two other ports. Considering the structure's symmetries, we can conclude that this degradation is not due to the design but caused most likely by the fabrication and metallisation process. Compared with simulated results, measurements

have higher phase dispersion. But performances reached over a bandwidth of about 3 GHz are acceptable for most applications. This point is addressed in the next section as we investigate the impact of amplitude and phase dispersion when the proposed matrix is used to feed a 4-element linear array antenna.

4. RADIATION PATTERNS

We use the measured amplitudes and phases of the proposed Butler matrix to evaluate the beam-patterns radiated by a 4-element linear array antenna defined analytically. The field pattern of the elementary radiator is modelled by the following formula:

$$E(\theta) = \cos(\theta)^{1.3} \tag{2}$$

This approximates the radiation pattern of a standard square-patch microstrip antenna, which is a simple and common elementary radiator design in printed planar array antennas. Neglecting coupling effects and using linear array factor formulation, we compute the radiation patterns when the 4-element linear array (with an array spacing of $0.6\lambda_0$) is fed by the measured matrix. The results are reported in Figure 22 at the center frequency. Each arithmetic phase progression produces a different beam pointing. Pointing directions achieved with measured data are respectively -12, $+30.8$, -31 and $+12°$. Theoretical values are -10, $+30$, -30 and $+10°$, resulting in a worst case pointing error of 2°. To study the beam pointing variation versus frequency, the same considerations are taken into account

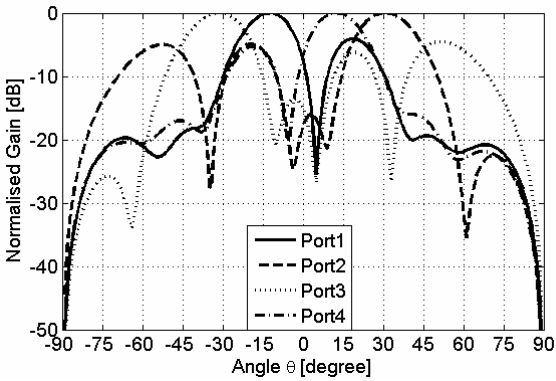

Figure 22. Simulated radiation patterns based on measured beam forming matrix performances at 12.5 GHz.

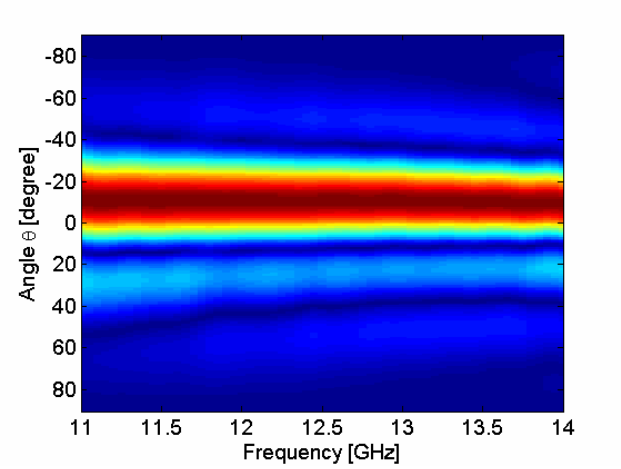

Figure 23. Variation of beam direction with frequency for port 1.

over the band 11–14 GHz. The results are reported in Figure 23 for port 1. The beam pointing deviation is of about 1° over the considered bandwidth. For port 2 this variation increases and beam pointing varies between 31 and 38° over the considered bandwidth. This variation could be anticipated. It is due to the fact that a constant phase difference is set over frequency. A true-time delay design is required to avoid this beam squint, but over the considered frequency bandwidth the beam squint observed remains acceptable for most applications.

5. CONCLUSIONS

A 4×4 Butler matrix has been designed in Ku-band with a central frequency of 12.5 GHz. Based on SIW technology, the proposed system has the advantages of low cost, light weight and ease of fabrication and integration. The elementary building blocks are designed for wideband operation and associated to evaluate the overall matrix performances. A 3 dB coupler as well as a 0 dB coupler (crossover) in SIW technology are proposed, designed for wideband operation around 12.5 GHz and fabricated using a standard PCB process. The measured results show good agreement with the designed and simulated results, with good operation observed over more than 24% relative bandwidth (3 GHz bandwidth centered at 12.5 GHz). The elementary components even have wider bandwidth operation (up to 35% frequency bandwidth for the 3 dB coupler), which make them really attractive even for other networks' design.

The proposed Butler matrix has better bandwidth than the state-of-art identified while maintaining single layer design, thus facilitating manufacturing aspects. Investigations presented in this paper also demonstrated the potential of such a matrix in association with a linear array antenna.

ACKNOWLEDGMENT

The authors are grateful to S. Dubé. J. Gauthier, T. Antonescu and J.-S. Décarie of the Poly-Grames reserach center, Ëcole Polytechnique de Montréal, for there technical assistance. The authors also want to thank the natural sciences and engineering research council of Canada (NSERC), the Fonds Québecois de la Recherche sur la Nature et les Technologies (FQNRT) and the Centre National d'Etudes Spatiales (CNES) for there financial support to this project.

REFERENCES

1. El Zooghby, A., "Potentials of smart antennas in CDMA systems and uplink improvements," *IEEE Antennas and Propagation Magazine*, Vol. 43, No. 5, 172–177, Oct. 2001.
2. Godara, L. C., "Application of antenna arrays to mobile communications. Part II: Beam-forming and direction-of-arrival considerations," *Proceedings of the IEEE*, Vol. 85, No. 8, 1195–1245, Aug. 1997.
3. Cladwell, F., J. S. Kenney, and I. A. Ingram, "Design and implementation of a switched-beam smart antenna for an 802.11b wireless access point," *Radio and Wireless Conference (RAWCON 2002)*, 55–58, 2002.
4. Polegre, A. M., G. Caille, L. Boyer, and A. Roederer, "Semi-active conformal array for ESA's GAIA mission," *IEEE AP-S International Symposium*, Vol. 4, 4108–4111, Jun. 2004.
5. Egami, S. and M. Kawai, "An adaptive multiple beam system concept," *IEEE Journal on Selected Areas in Communications*, Vol. 5, No. 4, 630–636, May 1987.
6. Rotman, W. and R. Turner, "Wide-angle microwave lens for line source applications," *IEEE Transactions on Antennas and Propagation*, Vol. 11, No. 6, 623–632, Nov. 1963.
7. Shelton, J. P., "Focusing characteristics of symmetrically configured bootlace lenses," *IEEE Transactions on Antennas and Propagation*, Vol. 26, No. 4, 513–518, Jul. 1978.

8. Herd, J. S. and D. M. Pozar, "Design of a microstrip antenna array fed by a Rotman lens," *IEEE AP-S International Symposium*, Vol. 22, 729–732, Jun. 1984.
9. Hall, P. S. and S. J. Vetterlein, "Review of radio frequency beamforming techniques for scanned and multiple beam antennas," *Proceedings of the IEEE*, Vol. 137, No. 5, 293–303, Oct. 1990.
10. Blass, J., "Multidirectional antenna, a new approach to stacked beams," *IRE International Conference Record*, Vol. 8, Part 1, 48–50, Mar. 1960.
11. Allen, J. L., "A theoretical limitation on the formation of lossless multiple beams in linear arrays," *IEEE Transactions on Antennas and Propagation*, Vol. 9, No. 7, 350–352, Jul. 1961.
12. White, W. D., "Pattern limitations in multiple-beam antennas," *IRE Transactions on Antennas and Propagation*, Vol. 10, No. 4, 430–436, Jul. 1962.
13. Butler, J. and R. Lowe, "Beam forming matrix simplifies design of electronically scanned antennas," *Electronic Design*, Vol. 9, 170–173, Apr. 1962.
14. Moody, H. J., "The systematic design of the Butler matrix," *IEEE Transactions on Antennas and Propagation*, Vol. 12, No. 6, 786–788, Nov. 1964.
15. He, J., B.-Z. Wang, Q.-Q. He, Y.-X. Xing, and Z.-L. Yin, "Wideband X-band microstrip Butler matrix," *Progress In Electromagnetics Research*, Vol. 74, 131–140, 2007.
16. Accatino, L., F. Muoio, B. Piovano, G. Caille, and M. Mongiardo, "CAD of waveguide Butler matrices including mechanical and thermal constraints," *31st European Microwave Conference (EuMC 2001)*, 1–4, Sep. 2001.
17. Koubeissi, M., C. Decroze, T. Monediere, and B. Jecko, "A new method to design a Butler matrix with broadside beam: Application to a multibeam antenna," *Microwave and Optical Technology Letters*, Vol. 48, No. 1, 35–40, Jan. 2006.
18. Deslandes, D. and K. Wu, "Integrated microstrip and rectangular waveguide in planar form," *IEEE Microwave and Guided Wave Letters*, Vol. 11, No. 2, 68–70, 2001.
19. Wu, K., D. Deslandes, and Y. Cassivi, "The substrate integrated circuits — A new concept for high-frequency electronics and optoelectronics," *TELSIKS'03*, Vol. 1, 3–10, Nis, Yugoslavia, Oct. 2003.
20. Ismail, A., M. S. Razalli, M. A. Mahdi, R. S. A. Raja Abdullah, N. K. Noordin, and M. F. A. Rasid, "X-band trisection

substrate-integrated waveguide quasi-elliptic filter," *Progress In Electromagnetics Research*, Vol. 85, 133–145, 2008.

21. Shen, W., X.-W. Sun, W.-Y. Yin, J.-F. Mao, and Q.-F. Wei, "A novel single-cavity dual mode substrate integrated waveguide filter with non resonating node," *IEEE Microwave and Wireless Components Letters*, Vol. 19, No. 6, 368–370, Jun. 2009.
22. Henry, M., C. E. Free, B. S. Izqueirdo, J. C. Batchelor, and P. Young, "Millimeter wave substrate integrated waveguide antennas: Design and fabrication analysis," *IEEE Transactions on Advanced Packaging*, Vol. 32, No. 1, 93–100, Feb. 2009.
23. Cassivi, Y., D. Deslandes, and K. Wu, "Substrate integrated waveguide directional couplers," *Asia-Pacific Microwave Conference*, Vol. 3, 1409–1412, 2002.
24. Hao, Z. C., W. Hong, J. X. Chen, H. X. Zhou, and K. Wu, "Single-layer substrate integrated waveguide directional couplers," *IEE Proceedings — Microwave, Antennas and Propagation*, Vol. 153, No. 5, 426–431, Octo. 2006.
25. Djerafi, T. and K. Wu, "Super-compact substrate integrated waveguide cruciform directional coupler," *IEEE Microwave and Wireless Components Letters*, Vol. 17, No. 11, 757–759, Nov. 2007.
26. Djerafi, T., J. Gauthier, and K. Wu, "Quasi-optical cruciform substrate integrated waveguide (SIW) coupler for millimeter-wave systems," *IEEE MTT-S International Microwave Symposium Digest (MTT)*, 716–719, 2010.
27. Labay, V. A. and J. Bornemann, "*E*-plane directional couplers in substrate-integrated waveguide technology," *Asia-Pacific Microwave Conference*, 1–3, 2008.
28. Ali, A., H. Aubert, N. J. G. Fonseca, and F. Coccetti, "Wideband two-layer SIW coupler: Design and experiment," *IET Electronics Letters*, Vol. 45, No. 13, 687–689, Jun. 2009.
29. Yamamoto, S., J. Hirokawa, and M. Ando, "A beam switching slot array with a 4-way Butler matrix installed in single layer post-wall waveguide," *IEICE Transactions on Communications*, Vol. E86-B, No. 5, 1653–1659, May 2003.
30. Djerafi, T., N. J. G. Fonseca, and K. Wu, "Architecture and implementation of planar 4×4 Ku-band Nolen matrix using SIW technology," *Asia-Pacific Microwave Conference*, 16–20, Dec. 2008.
31. Sbarra, E., L. Marcaccioli, R. V. Gatti, and R. Sorrentino, "A novel Rotman lens in SIW technology," *European Radar Conference*, 236–239, 2007.

32. Ali, A., N. Fonseca, F. Coccetti, and H. Aubert, "Novel two-layer broadband 4×4 Butler matrix in SIW technology for Ku band applications," *Asia-Pacific Microwave Conference*, 1–4, Dec. 2008.
33. European Cooperation for Space Standardization (ECSS), "Space engineering — Multipaction design and test," Vol. ECSS-E-20-01A, May 5, 2003.
34. Wolk, D., C. Vicente, H. L. Hartnagel, M. Mattes, J. R. Mosig, and D. Raboso, "An investigation of the effect of fringing fields on multipactor breakdown," *Workshop on Multipactor, RF and DC Corona and Passive Intermodulation in Space RF Hardware*, 93–99, Sep. 2005.
35. Cheng, Y. J., K. Wu, and W. Hong, "Power handling capability of substrate integrated waveguide interconnects and related transmission line systems," *Transactions on Advanced Packaging*, Vol. 31, No. 4, 900–909, 2008.
36. Wight, J. S., W. J. Chudobiak, and V. Makios, "A microstrip and stripline crossover structure," *IEEE Transactions on Microwave Theory and Techniques*, Vol. 24, No. 5, 270, 1976.